

Optimization Study and Validation of Gas Extraction Parameters Based on Heat-Fluid-Solid Coupling in Coal Seam

Minbo Zhang^{a,b}, Jin Yan^{a,*}, Ziyi Zhong^a, Zichao Wang^a, and Shilong Zhang^a

^aXingfa School of Mining Engineering, Wuhan Institute of Technology, Wuhan, 430074 China

^bJizhong Energy Resources Co., Ltd., Xingtai, 054000 China

*e-mail:yanjin19982001@163.com

Received August 8, 2023; revised September 6, 2023; accepted September 27, 2023

Abstract—In order to optimize the arrangement parameters of gas extraction in the downhole layer, the transport level of gas-containing coal was studied through industrial tests and low-temperature liquid nitrogen tests, and the heat-fluid-solid coupling model of the coal-rock deformation field, gas seepage and diffusion field, and temperature field was established, and numerically solved by using COMSOL. The optimal bore-hole diameter was determined by the single-hole gas extraction capacity, effective radius and extraction impact radius, based on which the superimposed extraction mechanism of neighboring boreholes and the change of gas extraction capacity under multi-hole extraction were studied, and the spacing of boreholes was finally determined. The study shows that: the test coal samples have high adsorption level of gas, the pressure difference between matrix and fissure under the influence of Klinkenberg effect leads to the decrease of gas seepage rate and extraction to a fixed value, the decreasing trend of coal body temperature decreases with the increase of extraction time, the decreasing rate of coal body permeability rises with the increase of attenuation coefficient, and the decreasing rate of gas extraction is accelerated accordingly. The reasonable drill hole diameter of 172403 working face in Dashucun Mine is 114mm, and the spacing of the holes is 6m, which has a good effect of on-site extraction and ensures the safe production of the mine and the sustainable development of the resources.

Keywords: Gas extraction, Heat-fluid-solid coupling, Gas accurate hole placement, Numerical simulation, Engineering Practice

DOI: 10.3103/S0361521923340013

INTRODUCTION

At present, domestic and foreign coal mines are gradually entering the deep mining state, and the increase of mining intensity leads to the decrease of permeability of coal seams and is accompanied by the problems of gas protrusion accidents and hydrogeological disasters [1–3]. The gas extraction is an effective method to prevent and control the gas herniation accidents and disasters, through the numerical simulation software to grasp the gas transport law can provide an optimal solution for on-site extraction, which is of practical significance to strengthen the gas extraction and prevention of disasters [4, 5]. In the extraction process, the flow of gas is affected by the deformation of coal and rock body, fluid movement, temperature change and other factors, which is the performance of the multi-field coupling effect of stress field, seepage field and temperature field [6].

In order to distinguish the seepage-diffusion relationship between coal matrix and fissure system, Li [5] investigated the multi-scale microscopic characteristics of different ranks of coal bodies through HPMT,

SEM, and low-temperature liquid nitrogen tests, which laid the foundation for the subsequent establishment of coal seam coupling models. By studying the mechanism of action between coal and stored CO₂, Liu [6] obtained the main reason for the change of porosity of coal body, revealed the law of action between the action force and microstructure of coal body, and contributed to the study of the equation of permeability and stress change of coal body. Liao [7] used liquid carbon dioxide phase change fracturing to improve the permeability of coal seams, which will help the study of coal mechanical damage and porosity equations by investigating the changes in the number of different pore fracture volumes after fracturing. Cheng [8] used the mathematical model of the working face gas source outflow law and gas transport to simulate the gas transport law in the overburden rock fissure area under the influence of mining, and designed a high-level directional long drilling technology for high-pressure gas extraction in the air-mining zone. Liu [9] established a coupled fluid-solid model of stress-damaged seepage based on COMSOL to

Table 1. Results of industrial analysis of raw coal at Dashu Village Mine

Coal Sample	M _{ad} (%)	A _{ad} (%)	V _{daf} (%)	V _{ad} (%)	FC _{ad} (%)
Large Coal	0.91	18.19	6.45	4.28	60.23

study the evolution law of the fissure field (seepage field) in the process of static blasting, and to solve the problem of fissure development of static blasting technology which is mostly calculated using empirical formulas in the coal mine site. Most of the coal mine sites use empirical formulas to calculate the fissure development of static blasting technology. Zhang [10] and others, in order to improve the gas extraction efficiency of the three soft coal seams, numerically simulated and analysed the mechanism of the hydraulic flushing fluid to strengthen the pumping by the method of combining FLAC 3D and COMSOL multi-physics field, and proposed a new type of discontinuous hydraulic flushing technology for the drilling holes in the slot. Yue [11] studied the relationship between anisotropy and the structure of the seam cuttings, and improved the degassing technology of coal seam slot drilling based on numerical simulation results and field test results. Wu [12] carried out numerical simulation of the plastic zone using COMSOL software, deduced the theoretical equation of the radius of the plastic zone, and put forward the anti-blowout hole equipment and the sealing technology of “two plugs and one injection”, and used phosphogypsum-based self-propelled hydraulic flushing technology to prevent the blowout hole. It proposed anti-drilling equipment and “two plugs and one injection” sealing technology, and used phosphogypsum-based self-produced gas-expanding paste material to seal the borehole, which improved the quality of sealing.

In the above studies, the techniques applied by the researchers in the field were derived based on the solution results of numerical simulation, but most of the studies regarded the coal seam as an isothermal system and did not establish a link between the matrix fracture pressure difference under the influence of the Klinkenberg effect and the amount of gas extraction. Therefore, the innovation of this paper is to introduce the dynamic diffusion coefficient, to study the mechanism of the matrix pore and fissure pressure difference under the influence of the Klinkenberg effect on the gas seepage rate and extraction, to explore the spatial and temporal patterns of permeability evolution under the attenuation of the dynamic diffusion coefficient, to improve the defects of the conventional study that treats the diffusion coefficient as a constant, and to establish a linkage between the effective stress and the adsorption and expansion stress at the same time. The coupled model of strain field, seepage field and temperature field of gas is established by considering effective stress, adsorption and expansion stress, and

Klinkenberg effect at the same time. Based on this model, the parameters of gas pre-pumping in the 172403 working face are optimised, and suitable hole diameters and spacing of holes are obtained, which provide a theoretical basis and guidance for the design of on-site pumping.

TEST ANALYSIS

Industrial Analysis of Coal Samples

All components of coal have an influence on gas adsorption capacity, with the greater the moisture content of the coal the lower the adsorption capacity. The ash content of the coal not only directly affects the storage content and reservoir properties, but also restricts the development of pores and fractures in the coal, which severely hinders gas transport. The lower the ash content in coal, the higher the degree of coal metamorphism and the stronger the gas adsorption capacity. As can be seen from Table 1, the coal samples from the Dashu Village Mine are anthracite, with a high degree of coalification and a high level of gas adsorption.

Isothermal Adsorption Curve Analysis

Figure 1 shows the isothermal adsorption curves of the coal samples from the Dashu Village Mine. The maximum sorption of the four groups of coal samples is 13.1245, 13.2679, 12.7842 and 12.6088 cm³ respectively, which indicates that the average maximum sorption of the Dashucun mine coal samples is 12.9435 cm³. According to the IUPAC classification, the sorption isotherms of the four groups of coal samples are biased towards Class IV, but are not identical. There is no overlap between the adsorption and desorption curves and they do not close at low relative pressures, indicating that the microporosity of the Dashucun mine coal samples is more developed and dominated by a sharp angle with one end closed, the pores of the coal samples are less connected. From Fig. 1 as a whole, the adsorption curve is always above the desorption curve, indicating that no new pore fissures were generated in the coal samples during the experiment. In the relative pressure range of 0 to 1.0, the coal adsorbed and desorbed nitrogen content increased and decreased rapidly, respectively, with the two curves being approximately steeply vertical, respectively. In the low pressure stage (relative pressure <0.45), nitrogen molecules begin to adsorb in a single molecular layer on the micro-pore pore walls as the relative pressure increases. At the medium to high pressure stage (0.45 to 0.9) there is a clear inflection point in the desorption curve, producing a hysteresis curve, which is also called hysteresis loop. At relative pressures >0.9, the adsorption curve rises steeply and the amount of adsorption increases abruptly, indicating that capillary coalescence is occurring in the pores at the same time as multi-molecular layer adsorption.

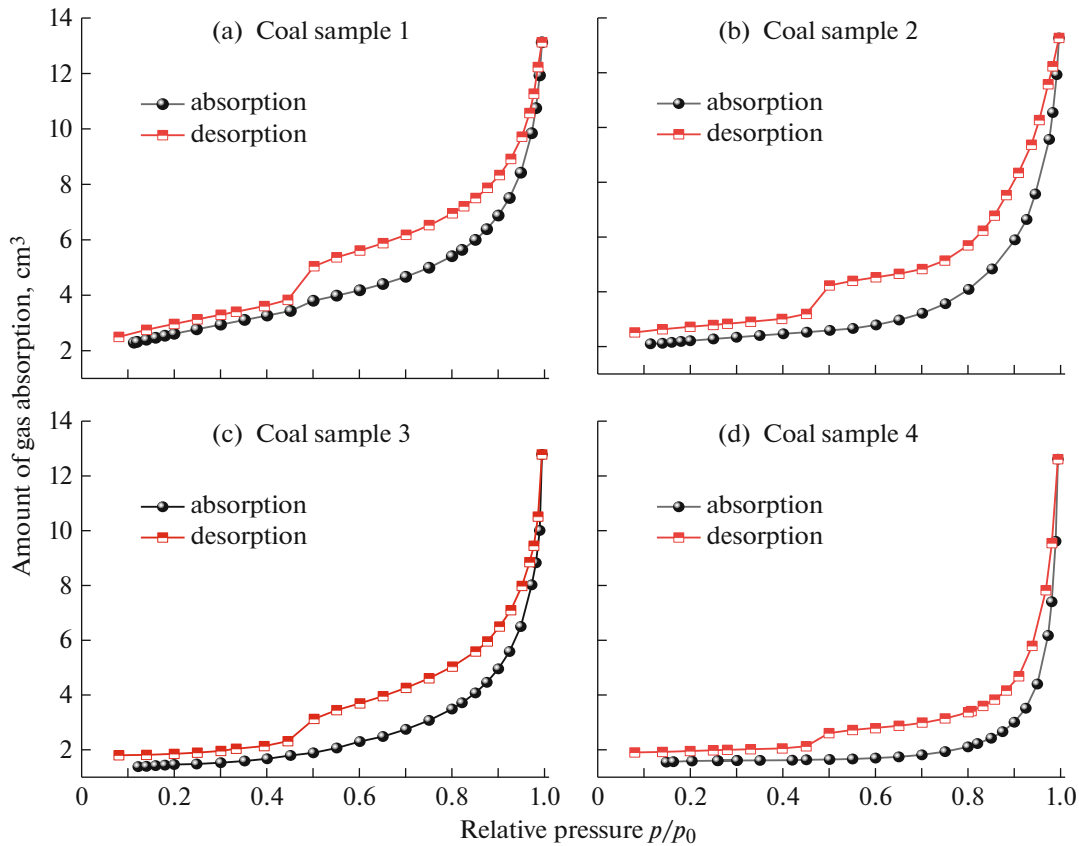


Fig. 1. Coal sample adsorption isotherms.

In this paper, the most common B.B. Hodot decimal division method was used to classify the coal pore type system, and the BJH theoretical model was used to calculate the model. Figure 2 shows the pore size distribution characteristics of the four groups of coal samples obtained from the experiment.

The pore size distribution data measured using the BJH method is generally chosen to be plotted using dV/dD , with the pore size distribution most concentrated at the peak of the curve in the graph. In general, pores below 100 nm in diameter, especially micropores, determine gas adsorption, storage and transport. The pore size distribution of all four groups of coal samples showed a single peak distribution, with the pore sizes concentrated in the 2–20 nm region, indicating that the gas adsorption capacity of the coal samples from the Dashucun Mine is mainly determined by the 2–20 nm micro-pores, which play a dominant role in the storage and transport of gas in the coal seam. The pore size distribution was most concentrated in the 3–5 nm interval, and the micro-pores in this interval contributed most to the surface area and pore volume.

COAL SEAM GAS HEAT-FLOW-SOLID COUPLING MODEL

The transport of gas in the coal seam is affected by many factors, and the following assumptions are made first: (1) the coal body endowed with gas is an ideal gas, and the adsorbed gas satisfies Langmuir theory. (2) coal body skeleton is linear elastic body, following the assumption of small deformation. (3) the coal contains only single-component gases. (4) the flow of gas through the cracks of the coal seam is in accordance with Darcy's law.

Modelling of Coal Porosity and Permeability Evolution

Considering the effect of effective stress and adsorbed expansion stress on the coal body skeleton [13], the porosity of the coal body with dual pore structure can be expressed by the following equation:

$$\varphi = \varphi_0 + \frac{\beta_f}{M}(p_f - p_{f0}) + \frac{\beta_m}{M}(p_m - p_{m0}) + \frac{a\rho_s RT}{MV_m} \ln \frac{1 + bp_0}{1 + bp} \quad (1)$$

Where φ and φ_0 are porosity and initial porosity, %; β_f and β_m are effective stress coefficients of fissure and

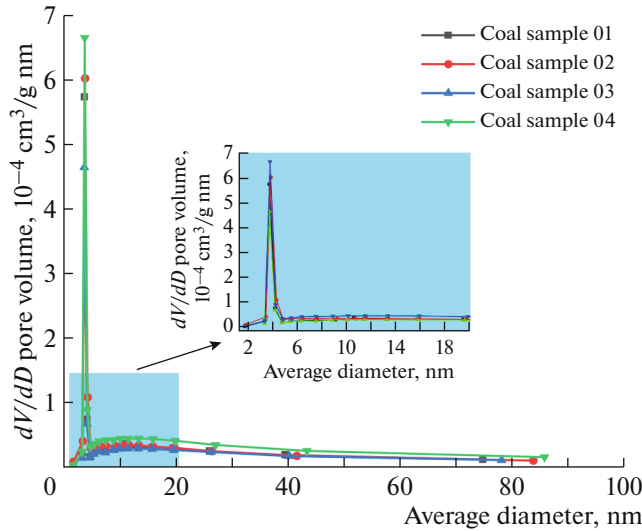


Fig. 2. Pore size distribution characteristics of coal samples.

matrix; p_f is fissure gas pressure, Mpa; p_m is matrix gas pressure, Mpa; and a is ultimate adsorption capacity, cm^3/g ; ρ_s is the true density of the coal body, kg/m^3 ; T is the temperature of the coal seam, K; b is the adsorption equilibrium constant, Mpa^{-1} ; p is the coal seam gas pressure, Mpa; M is the coal axial confinement modulus, Mpa; K is the coal bulk modulus, MPa.

There is a cubic relationship between coal permeability and porosity [14, 15], i.e., the coal permeability can be expressed as:

$$\frac{k}{k_0} = \left(\frac{\phi}{\phi_0} \right)^3. \quad (2)$$

Where k , k_0 denote the permeability and initial permeability, mD, respectively.

The Klinkenberg effect exists in the flow of gases through porous media, and the following relationship exists between the effective permeability and absolute permeability of gas [16–19]:

$$k_e = k \left(1 + \frac{c}{p_f} \right). \quad (3)$$

Where k_e is the effective permeability of gas transport, mD; c is the Klinkenberg coefficient, generally taken as 0.251; p_f is the fissure gas pressure, Mpa.

Bringing (3) into (2) equation, the evolution formula of effective permeability of coal seam under the influence of Klinkenberg effect can be obtained:

$$\frac{k}{k_0} = \left(\frac{\phi}{\phi_0} \right)^3 = \left\{ 1 + \frac{\beta_f}{M\phi_f} (p_f - p_{f0}) + \frac{\beta_m}{M\phi_{f0}} (p - p_0) + \frac{a\rho_s RT}{MV_m\phi_0} \ln \frac{1 + bp_0}{1 + bp} \right\}^3 \cdot \left(1 + \frac{c}{p_f} \right). \quad (4)$$

Where p_{f0} indicates the initial fracture pressure, Mpa; p_{m0} is the initial substrate pressure, Mpa.

Substrate Gas Transport Equation

The amount of gas per unit volume of coal matrix is given by the following equation [20]:

$$m_m = \frac{abp_m\rho_c M_C}{(1 + bp_m)V_m} + \phi_m \frac{M_C p_m}{RT}. \quad (5)$$

Where m_m denotes the gas content in the coal matrix, kg/m^3 ; ρ_c is the pseudo-density of the coal body, kg/m^3 ; M_C is the molar mass of methane, kg/mol ; and V_M is the molar volume of the gas at standard conditions, L/mol. ϕ_m is the initial porosity.

Most of the studies treated the diffusion coefficient as a constant, but the diffusion coefficient showed an attenuation with time, so the attenuation coefficient was introduced to calculate the diffusion coefficient [21–23]:

$$D_t = D_0 \exp(-\lambda t). \quad (6)$$

Where D_t is the dynamic diffusion coefficient, m^2/s ; D_0 is the coal seam gas diffusion coefficient, m^2/s ; λ is the attenuation coefficient, s^{-1} ; t is the extraction time, d.

The coal seam matrix system and fissure system exchange mass under pressure difference [22], and the equation of change of gas pressure in the matrix pores is:

$$\frac{\partial p_m}{\partial t} = - \frac{3\pi^2 V_m (1 + bp_m)^2 (p_m - p_f) D_t}{L^2 [ab\rho_c RT + \phi_m V_m (1 + bp_m)^2]}. \quad (7)$$

Where L is the spacing of the coal body fissures, m.

Fissure Gas Seepage Equation

Gas flow in a fracture system follows Darcy's law [17]:

$$v_f = - \frac{k}{\mu} \nabla p_f. \quad (8)$$

Where v_f is the seepage velocity, m/s; μ denotes the kinetic viscosity coefficient of the gas, which is generally taken as $1.0810^{-5} \text{ Pa} \cdot \text{s}$. ∇p_f indicates the fracture pressure gradient, kPa/m.

From the law of conservation of mass, the change in the amount of gas in the fissure is the value of matrix diffusion minus the inflow of free gas from the fissure into the borehole [24]:

$$\frac{M}{RT} \frac{\partial \phi_f}{\partial t} = Q_m (1 - \phi) - \nabla \cdot \left(\frac{M}{RT} p_f v_f \right). \quad (9)$$

Where Q_M is the mass exchange law per unit volume of coal matrix with the fracture system, $\text{kg}/(\text{m}^3 \cdot \text{s})$.

Associating equations (8), (9), an expression for the variation of gas pressure with time in the fissure can be obtained:

$$\begin{aligned} & \phi_f \frac{\partial p_f}{\partial t} + p_f \frac{\partial \phi}{\partial t} \\ &= \frac{3\pi^2 D_t (1 - \phi_f)}{L^2} \cdot (p_m - p_f) + \nabla \left[\frac{k}{\mu} p_f \nabla p_f \right]. \end{aligned} \quad (10)$$

Deformation Control Equation of Coal Rock Body

Considering the effect of adsorbed expansion stress on the coal skeleton [16], the Biot coefficient is quoted into the effective stress equation:

$$\sigma_{ij}^k = \sigma_{ij} - (\beta_f p_f + \beta_m p_m + \sigma_a) \delta_{ij}. \quad (11)$$

Where σ_{ij} is the effective stress on the coal body, Mpa; σ_a is the adsorbed expansion stress, Mpa; δ_{ij} is the Kronecker delta sign.

$$\begin{cases} \beta_f = 1 - \frac{K}{K_m} \\ \beta_m = \frac{K}{K_m} - \frac{K}{K_s} \end{cases} \quad (12)$$

$$\sigma_a = \frac{a \rho_s R T \ln(1 + b p_m)}{V_m}. \quad (13)$$

Where K_m is the coal matrix modulus, MPa; K_s is the coal skeleton modulus, MPa.

The joint equation (10), (11), (12), can be obtained Navier form of the coal body deformation equation:

$$\begin{aligned} & G u_{i,jj} + \frac{G}{1 - 2\nu} u_{i,jj} + \frac{2ab\rho_s R T}{3V_m(1 + bP)} P_{,i} \\ &+ (\phi P)_{,i} + \frac{2a\rho_s R \ln(1 + bP)}{3V_m} T_i + F_i = 0. \end{aligned} \quad (14)$$

Where $P_{,i}$ T_i represent the coupled terms of gas seepage and temperature field variations, respectively; $(\phi P)_{,i}$ is the gas adsorption-desorption term.

Equation of Control for Coal Seam Temperature Field

The coal seam gas transport process is non-isothermal, i.e., there is heat exchange during gas desorption, desorption, and seepage [25–27]. Therefore, coal body temperature coupling needs to consider the effects of stress field and seepage field comprehensively:

$$\begin{aligned} & \eta \nabla^2 T + VQ = p_s C_v \frac{\partial T}{\partial t} \\ &+ T_0 \left(\frac{2a\rho_s R \ln(1 + bP)}{3V_m} + \frac{\partial \phi}{\partial T} P \right) \frac{\partial \epsilon_v}{\partial t}. \end{aligned} \quad (15)$$

Where C_v is the constant volume specific heat capacity; η is the thermal conductivity of the coal body. Q is the gas content of the coal seam, kg/m^3 . T_0 is the initial temperature of the coal seam, K. ϵ_v is the volumetric strain of the coal body.

In summary, the coupling equation (7), (10), (14), (15) constitutes the heat–fluid–solid coupling equation of coal and gas, which reveals the change process between the internal microscopic transport process of the coal body and the change of permeability and porosity, the deformation of the coal body, as well as the temperature of the coal seam, and its multi-field physical coupling relationship is shown in Fig. 3.

NUMERICAL SIMULATION SOLUTION

Numerical Modelling and Parameters

In this paper, numerical simulation is carried out with Dashucun coal mine as an engineering example, the gas content is 10.2~12.4 m^3/t , and the coal seam has the risk of protrusion, which needs to optimise the existing extraction technology. As shown in Fig. 4, the model size is $50 \times 40 \times 4$ m, and the drill hole is located in the middle of the coal seam with a length of 50 m. The upper part of the model is a stress boundary, the lower part is a fixed boundary; the left, right and back sides are rolling boundaries, and the absolute pressure of the roadway in the coal seam is 0.1 Mpa.

In order to better study the change of the gas transport law of the borehole, a reference surface is intercepted on the cross-section YZ with X as the coordinate of 30 m. The reference surface is located in the middle of the two-dimensional cross-section, as shown in Fig. 5. As shown in Fig. 5, the gas extraction borehole is located in the middle of the two-dimensional cross-section, the borehole diameter is 75 mm, and four observation points are set every 0.5 m on the right side of the borehole. The top of the coal seam is subjected to a loading pressure of 10 MPa, the bottom is a fixed constraint, and the left and right ends are rolling boundaries. The pressure boundary is around the borehole, and the rest of the boundaries are set as zero-flow boundaries. The parameters used in the simulation are derived from the field engineering measurements and partly referred to authoritative related research papers [28–30], and the specific parameters are shown in Table 2.

Research on the Law of Gas Extraction and Transport

From the study [16], it is clear that the permeability of the coal body is controlled by the dual mechanism of effective stress and matrix adsorption, showing regular dynamic changes with the time of extraction. As gas extraction proceeds, matrix adsorbed gas is continuously desorbed, and a small amount of free gas within the matrix moves into the fissure, and is subse-

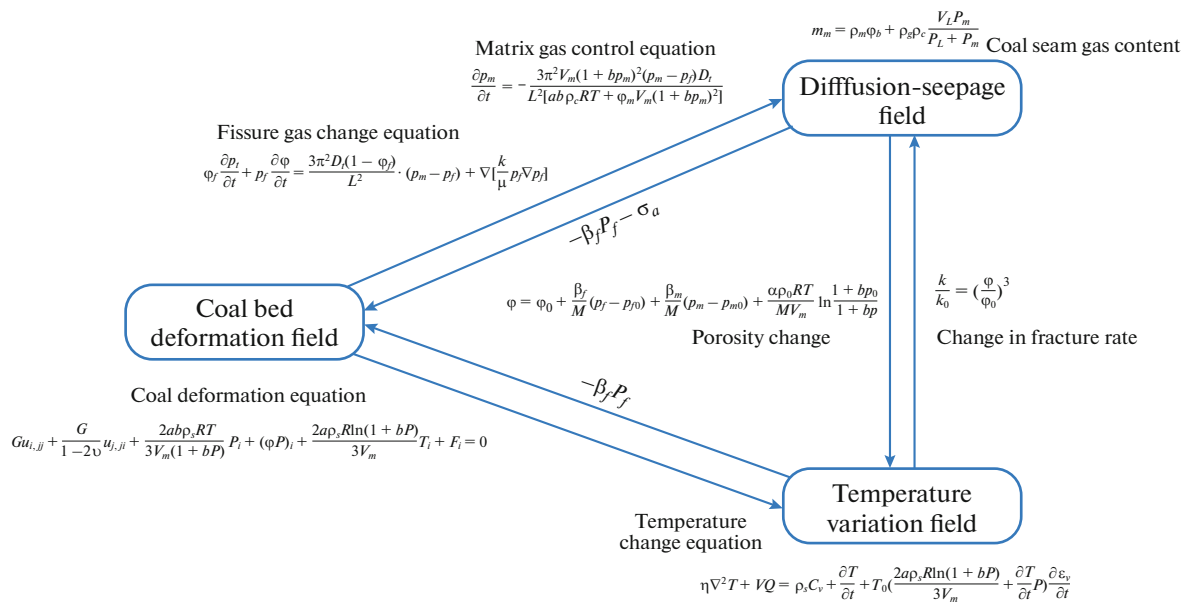


Fig. 3. Heat-fluid-solid coupling physical relationship diagram.

quently continuously discharged from the coal seam. In this process, the increase in effective stress leads to a decrease in the permeability of the coal body, and matrix contraction leads to an increase in the amount of matrix gas diffusion, resulting in an increase in the permeability of the coal body, and the change in the permeability of the coal body is a result of the competition between the adsorption expansion and deformation of the coal matrix and the effective stress. As can be seen from Fig. 6, the reasons for this phenomenon are: with the gas extraction, the pressure around the borehole is decreasing, even if the effective stress of the coal seam increases, but the matrix contraction effect around the borehole dominates; the larger the diffusion attenuation coefficient is, the greater the matrix gas diffusion resistance is at a distance from the borehole, and the matrix contraction effect decreases, and the permeability decreases at a faster rate, which results in the slowing down of gas seepage and the decrease of the amount of gas extracted. This phenomenon reflects the fact that considering the

dynamic diffusion coefficient. This phenomenon reflects the necessity of considering the dynamic diffusion coefficient, and provides a theoretical basis for the optimisation of extraction parameters.

Figure 7 shows the curves of gas seepage velocity of the fissure and gas extraction volume with time at observation points A1, A2, A3 and A4. The pressure difference between the fissure and matrix is the largest at the early stage of extraction, corresponding to the largest amount of diffused gas in the matrix. Therefore, the pressure difference between the fissure and the outside of the borehole increases, and the gas is continuously discharged from the fissure to the outside of the borehole, and the seepage velocity rises sharply to the peak value. As the extraction time increases, the Klinkenberg effect leads to an increase in the molecular thickness of the fissure surface, the mass source of the coal matrix diffused into the fissure decreases, and the pressure difference gradually decreases and is fixed to a stable value. At this time, the mass source provided by the matrix is not enough to supplement the gas flowing out of the fissure, resulting in a decrease in the pressure difference

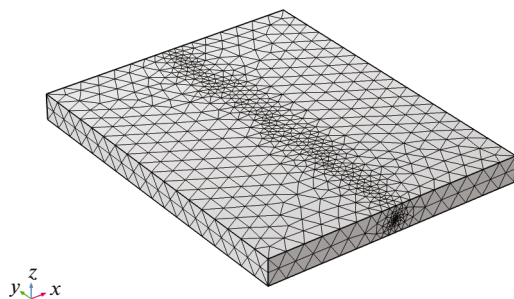


Fig. 4. Geometric model of gas extraction.

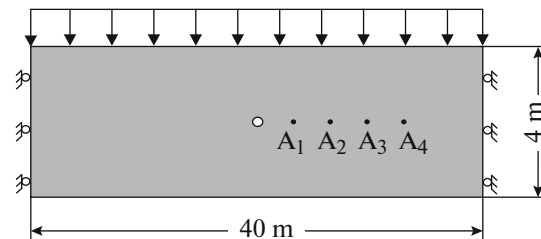


Fig. 5. Location of monitoring points in YZ section.

between the fissure and the outside of the borehole, and the seepage rate continues to slow down to a fixed value. From the change curve of gas extraction quantity, it can be obtained that: at the beginning of extraction, the gas extraction rate decreased rapidly from 41.8 to 5.02 m³/d, and then began to decrease steadily until it stabilised at 1.90 m³/d.

Coal Seam Temperature Change Law

From the study [23], it is clear that the coal seam temperature decreases continuously with the time of extraction. Figure 8 shows the isotherm map of coal seam temperature change under different extraction time, and it can be seen from the change of the map that the coal seam temperature isotherm is constantly spreading from the borehole to the distant part of the coal seam with the increase of time. When the extraction time is the same, the temperature of the coal seam shows an increasing trend from the centre of the borehole to the outside, and the temperature increases with the increase of the distance from the borehole, and the temperature of the coal seam farther away from the extraction borehole is close to the initial temperature value. When $t = 30$ d, the temperature at 5m from the centre of the drill hole is 276.15 K; when $t = 60$ d, the temperature of the coal seam at this point is 274.95 K, and the temperature of the coal body decreases by 1.2 K; when $t = 90$ d, the temperature of the coal body is 274.25 K, and the temperature decreases by 0.7 K; and when $t = 120$ d, the corresponding temperature of the coal body is 273.75 K, and the temperature decreases by 0.5 K. It can be seen that the temperature of the coal body increases with the extraction time. Coal body temperature decreases

Table 2. Simulation parameters

Parameter	Value
Initial porosity φ_0	0.05
Initial permeability k_0/mD	0.2
borehole size d_0/m	0.75
Langmuir pressure P_L/MPa	1.2
Initial coal seam temperature T_0/K	295
Langmuir volume $V_L/\text{m}^3 \cdot \text{kg}^{-1}$	0.02
Apparent density of coal $\rho_s/\text{kg} \cdot \text{m}^3^{-1}$	1250
Klinkenberg factor c/MPa	0.76
Negative extraction pressure p_b/kPa	25
Limit adsorption deformation	0.006
Initial gas diffusion coefficient $D_0/\text{m} \cdot \text{s}^{-1}$	3.5×10^{-12}
Modulus of elasticity of coal K_m/MPa	2700
Poisson's ratio of coal ν	0.339
Fissure compression coefficient β_0/MPa^{-1}	0.02
Initial gas pressure of coal seam p_0/MPa	2

continuously with the increase of extraction time, and the decrease rate shows a slowing down trend.

Figure 9 shows the variation of the coal body temperature along the distance of the coal seam strike. It can be seen that with the increase of the distance from the centre of the borehole, the temperature of the coal seam increases continuously and remains constant after increasing to a certain value. When the temperature of the coal seam reaches the 295.15 K isotherm, the different pumping times corresponding to the distance from the centre of the borehole are shown

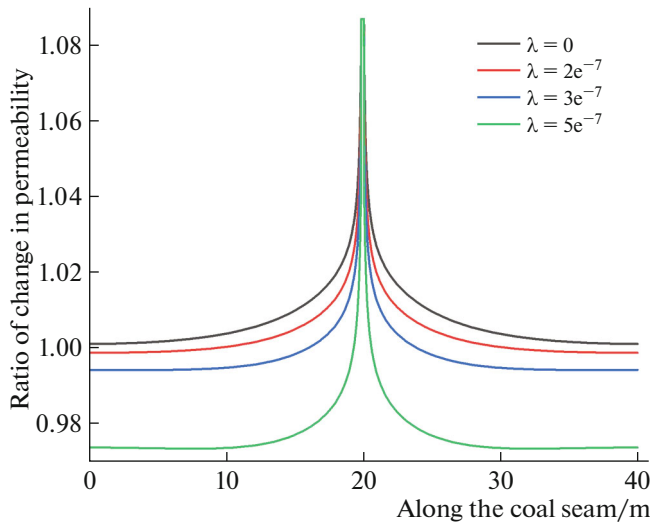


Fig. 6. Variation curve of coal seam permeability with diffusion coefficient.

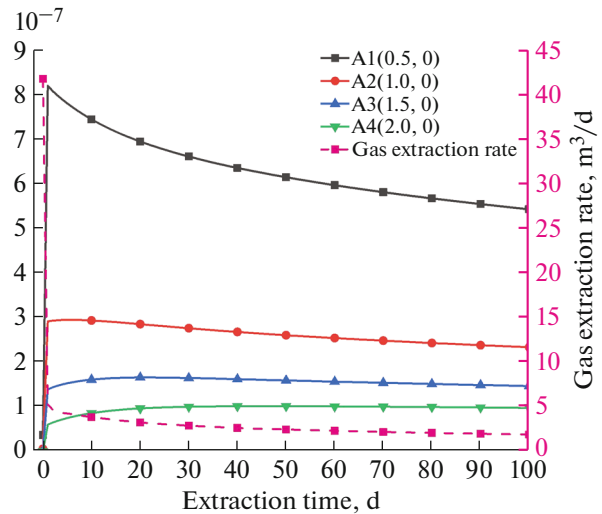


Fig. 7. Variation curves of seepage rate and gas extraction at observation point.

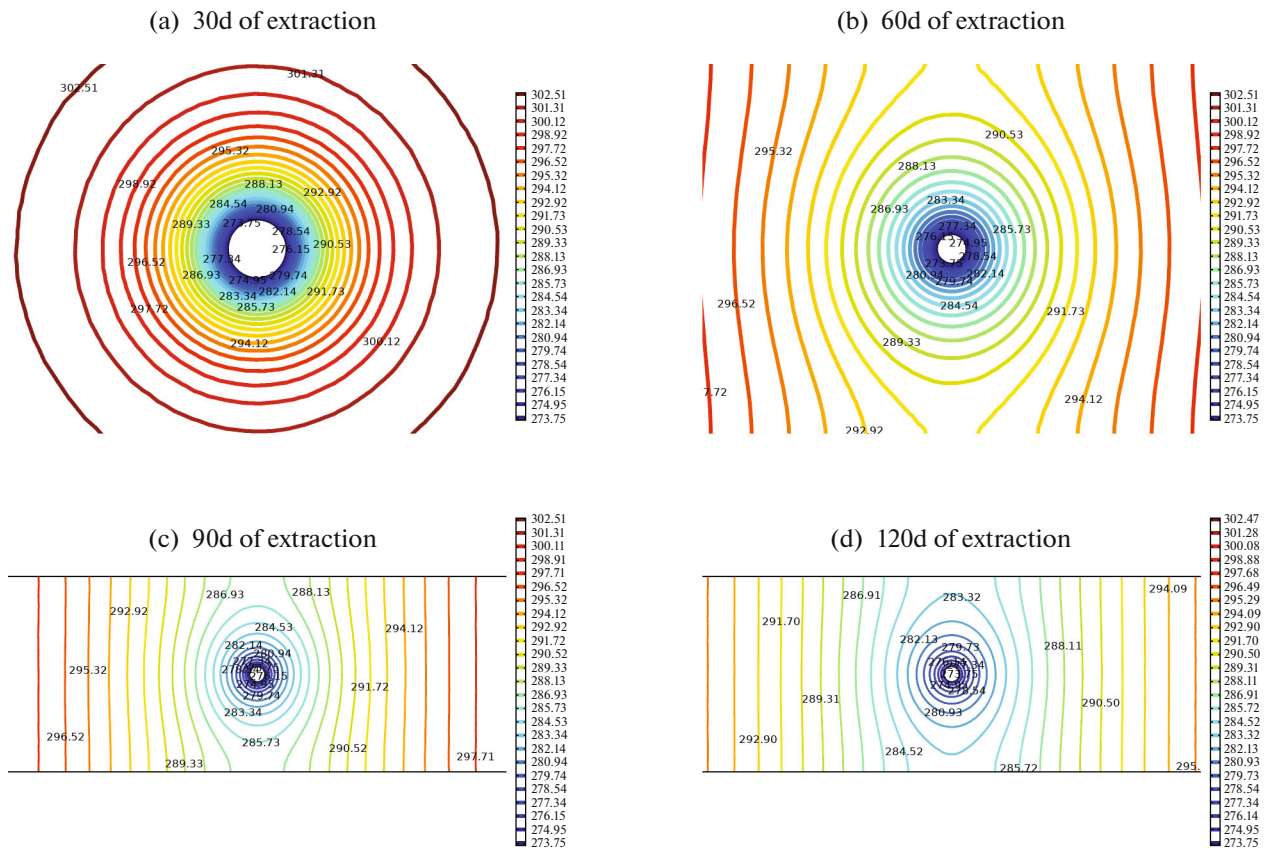


Fig. 8. Temperature contour plot around drill hole.

as follows: when pumping for 30d, the distance is. It can be seen that the temperature of the coal body is lower with the increase of this extraction time. This is because the adsorption and desorption of matrix gas need to consume a certain amount of heat, and the movement of fissure gas seepage has a certain thermal effect, at this time, the coal seam is a non-isothermal system, and the transport of gas continuously converts thermal energy into kinetic energy. At the same time, the external force acting on the coal rock layer also produces thermal effect. As the gas extraction process proceeds, the gas content of the coal seam decreases, and the reduction of gas pressure accompanied by the heat conduction of the coal body also leads to a decrease in the temperature of the coal seam. At the late stage of extraction, the gas pressure and content drop to a stable value, and the resistance of gas transport between matrix and fissure system increases, at this time, the thermal effect of the coal body is less, and the temperature of the coal seam reaches a stable value.

Figure 10 shows the influence curve of different initial temperatures on the effective extraction area, and it can be seen that the area of effective extraction area decreases with the increase of the initial temperature of the coal seam. In the initial period of 0–60 d,

the area of effective extraction area increases gently. After 60 d of mining, the effective extraction area increases rapidly to a stable value. After 120 d of extraction, the effective extraction area at $T_0 = 302$ K, 291 K and 280 K is 2.62, 4.15 and 9.11 m² respectively, and the initial temperature of the coal seam at 291 K has decreased by 54.5% compared with that at 280 K, and the extraction compliance area at 302 K has decreased by 36.9 and 71.2% compared with that at 291 and 280 K respectively, and the reduction rate decreases with the initial temperature of the coal seam. It can be seen that the high temperature coal seam is not favorable for gas extraction, and effective technical measures should be taken to reduce the temperature of coal seam before pre-extraction of coal seam, such as the use of wet drilling, water injection into the coal seam and other methods.

OPTIMISATION OF GAS EXTRACTION PARAMETERS

Rational Extraction Borehole Size Study

From the study [31], it can be obtained that the gas pressure around the borehole reaches 50% of the ini-

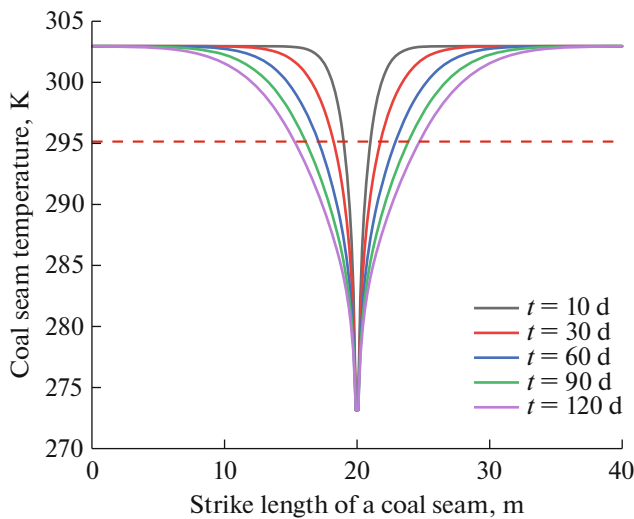


Fig. 9. Coal seam temperature variation curve.

tial gas content after a certain pre-extraction time is considered to be the compliance area. The study [19] takes into account the dynamic complexity of the site, and the area below 75% of the initial level is considered as the zone of influence of extraction.

Figure 10 shows the effective extraction radius and effective influence radius of the four hole diameters at 120 d. The effective extraction radius and effective influence radius of the drill holes increase with the increase of hole diameters. Among them, the growth rate of 114 mm borehole diameter is 25%, the fastest growth rate. Figure 11 shows the variation curves of gas extraction with hole diameter at different extraction times. During 0–50 d of extraction, the gas extraction decreased rapidly, and the decrease of gas extraction gradually decreased and stabilised at the late stage of extraction. The decrease rate of gas extraction increases with the increase of borehole diameter, and the decrease rates of gas extraction for 75, 94, 114, and 137 mm boreholes are 46.7, 47.8, 52.6, and 52.8%, respectively. The extraction effect of 75 mm and 94 mm boreholes is obviously inferior to the latter two types of boreholes, but the difference between the decrease rates of gas extraction in the 114 and 137 mm holes is relatively small. However, the difference in the decrease rate of gas extraction between 114 and 137 mm boreholes is relatively small, and the extraction effect is similar. When extracting gas from the working face, the use of larger boreholes will easily increase the difficulty of construction, and may result in collapsing holes, plugging holes, jamming and other phenomena. This not only causes waste of resources, but also increases the risk of gas protrusion. Therefore, considering the economic and safety factors and the extraction effect, it is more reasonable to choose the hole diameter of 114 mm, and the effective

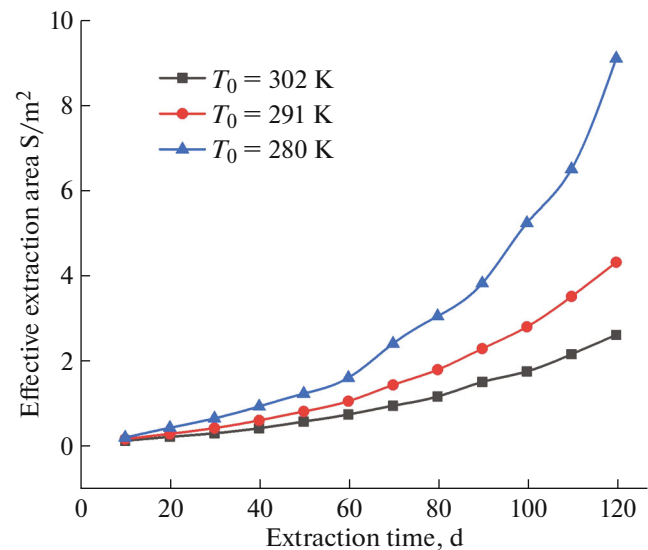


Fig. 10. Variation of effective extraction area with initial coal seam temperature.

extraction radius and the effective influence radius for 120 d of extraction are 2.16 and 7.8 m, respectively.

Study of Reasonable Hole Spacing

From the study [10–13], it can be seen that the working face is generally arranged with multiple drill holes for gas extraction, and there is a superposition effect between neighboring drill holes. The determination of the time distance of multi-drilling is mainly based on the gas extraction radius as a reference, the study [17] through field testing and verification, concluded that the effective extraction radius r area is the main area of gas pressure reduction in coal mines, and the effective influence radius R is the secondary area of gas pressure reduction in coal seams, and the reasonable spacing of drilling holes is in the range of $(2r, R + r)$. The superposition effect of gas extraction will cause the gas pressure at a point far away from the drill holes to be much larger than that between the drill holes, so that the extraction effect will be much larger than that under single-hole extraction. Therefore, based on the results of the previous study on the borehole diameters, drill holes #1, #2, and #3 were arranged to study the variation of gas pressure and gas extraction at intervals of 4 m, 6 m, and 8 m, respectively, as shown in Fig. 13, and the basic simulation parameters are the same as those in the previous study.

Figure 14 shows the cloud diagram of gas pressure variation at 120 d of gas extraction from different spaced boreholes. When the extraction time is the same, the pressure difference between the coal seam pressure and the negative pressure of the borehole extraction leads to the accumulation of gas gas farther away from the borehole. As a result, the gas pressure increases the further away from the borehole centre,

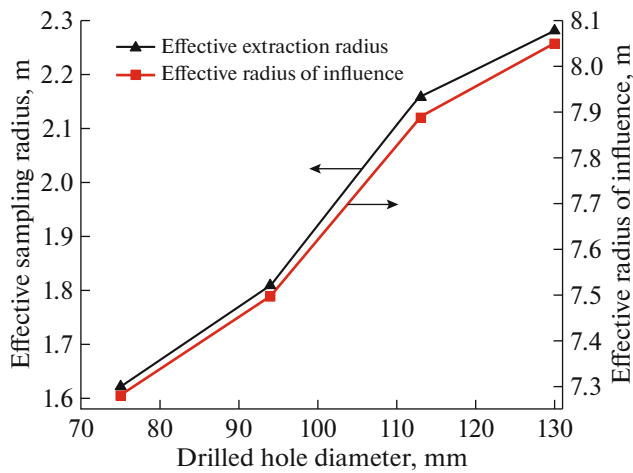


Fig. 11. Effective radius of gas extraction and effective radius of influence under different borehole diameters.

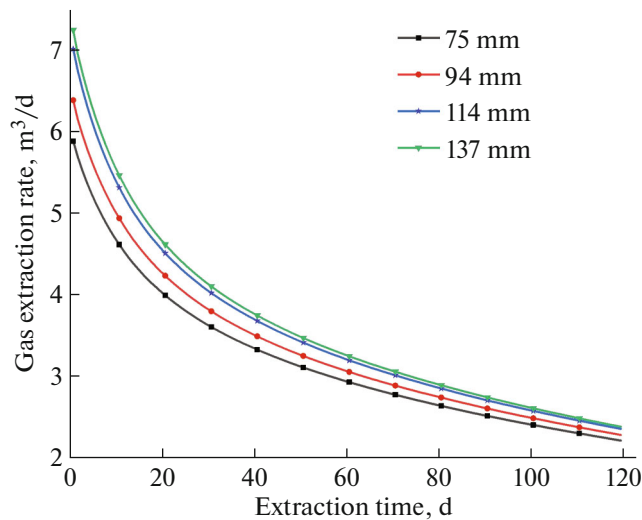


Fig. 12. Variation curve of gas extraction volume with time under different borehole diameters.

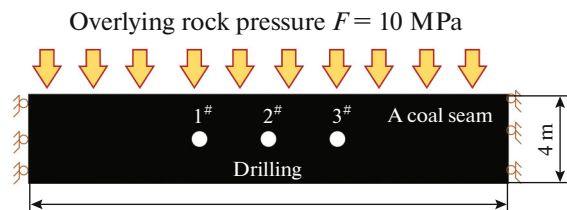


Fig. 13. Schematic diagram of multi-drilled hole geometry model.

and approaches the initial coal seam pressure at the farther borehole wall. With increasing extraction time, the gas pressure decreases. In the late stage of extraction, the resistance to gas diffusion increases, leading to a decrease in the amount of gas flowing into the fissure system, and the rate of gas decline gradually decreases, and the effect of gas extraction tends to stabilise. As can be seen from Fig. 14a, when the spacing is 4 m, a continuous low-pressure area is formed between the three boreholes, and at this time, the pressure values near the three boreholes are significantly smaller than those outside, which is because the distance between the boreholes is relatively close, and under the effect of the negative pressure of the boreholes and the pressure difference of the coal seam gas pressure, the gas in the low-pressure area has the fastest transport speed, and thus the pressure drop is the most significant. Figures 14b and 14c correspond to the spacing of 6 m and 8 m, the spatial distribution of gas pressure is basically similar to Fig. 14a. When the spacing is 6 m, the superposition effect between neighbouring boreholes is obvious, and the pressure drop area between the three boreholes is within the specified pressure range; when the spacing is 8 m, the degree of inward depression between neighbouring boreholes is larger, and the pressure drop area formed by the three boreholes appears to have an area that has not been reduced to less than 0.74 MPa, which indicates that the superposition effect generated by the arrangement of boreholes at the distance of 8 m is weaker, resulting in a situation where the extraction efficiency between neighbouring boreholes does not reach the level of 0.74 MPa. The pumping efficiency between the neighbouring drill holes is not up to the standard.

Figure 15 shows the relationship between the gas pressure at the centre position between adjacent drill holes and the gas extraction amount with the change of extraction time, when the extraction time is 120 d, the pressure at the centre position of the two drill holes of 4, 6 and 8 m decreases to 0.5, 0.6 and 0.8 MPa, respectively. when the extraction time is the same, the adjacent drill holes are subjected to the effect of the superposition effect between the drill holes, the smaller the drill holes spacing is, the smaller the gas pressure between the drill holes, and the smaller the value of the residual gas in the seam. The smaller the value of residual gas in the coal seam. The decrease rate of gas extraction slows down with the increase of hole spacing, and after 120 d of extraction, the gas extraction at 4, 6 and 8 m spacing is stable at 0.89, 1.21 and 1.39 m³/d, respectively. When the spacing of the drill holes is too small, the overlapping area of extraction and the construction volume of the holes increase, which raises the cost of the gas extraction. Considering the change of gas pressure and extraction volume, 4 m spacing will cause excess extraction overlapping zone and fast decay of gas extraction volume, 8 m spacing will make extraction appear “blank zone”,

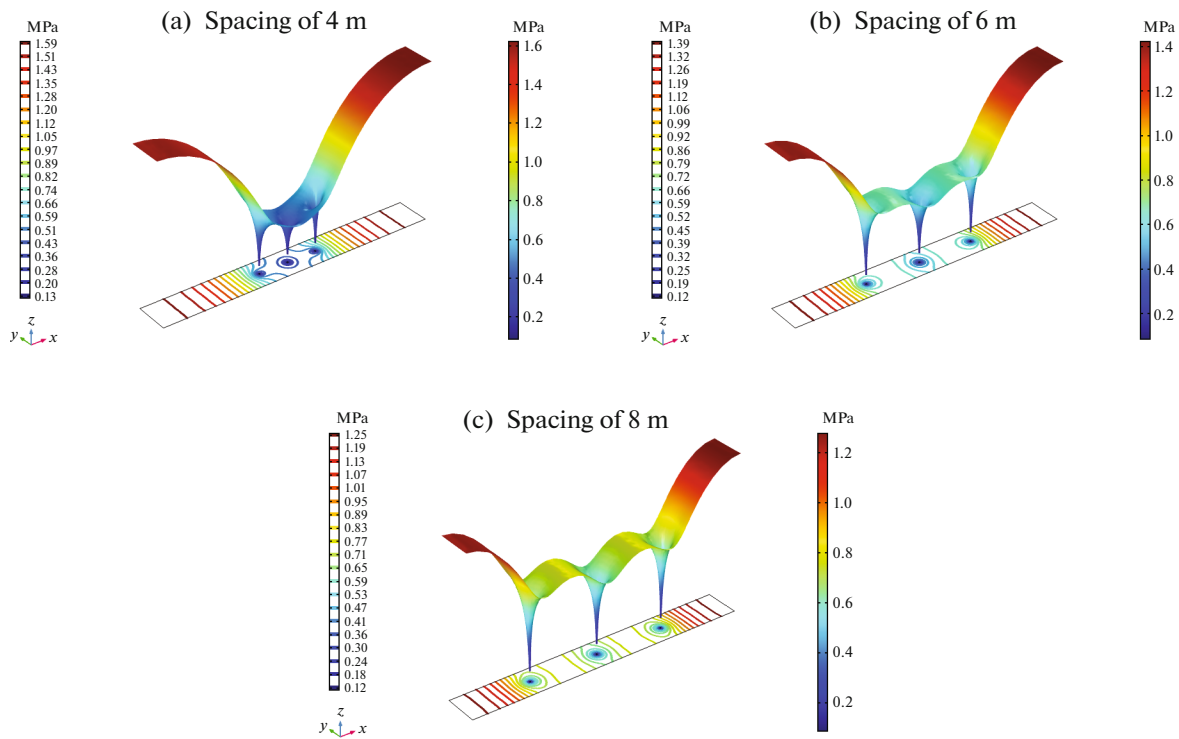


Fig. 14. Cloud map of gas pressure distribution under different drill hole spacing.

and the risk of coal seam protrusion is higher, so we choose to arrange the drilling holes with 6 m spacing.

Practical Verification of Coalbed Methane Mining

The parameters of regional gas extraction volume, pure extraction volume and extraction concentration of test 172403 working face (OPQRS) were statistically calculated, and the total extraction volume was 727814.5 m³ measured online and 719379.2 m³ measured manually from March 18, 2022 to September 13, 2022, and the automatic measurement and manual measurement data were compared. The error is less than 5% as stipulated in the Measures for Comprehensive Management of Coal Mine Gas in Hebei Province. The total extraction volume is based on the online measurement.

Based on the online metering data and the gas pre-pumping data of the test area and the adjacent area, the pure volume and concentration of gas extraction are plotted as shown in Figs. 16 and 17. From Fig. 16, it can be seen that the pure volume of gas extraction fluctuates upward with time, then stabilizes, and finally fluctuates downward. After the peak, the pure volume of extraction was decreasing until the final volume was 1.02 m³/min, and the average pure volume of extraction was 2.67 m³/min. In the early stage of extraction, the pure amount of gas in the adjacent area is the same as that in the (OPQRS) area, but as time passes, the pure amount of gas extraction in the

(OPQRS) area is obviously higher than that in the adjacent area, the peak pure amount of extraction in the adjacent area is only 3.40 m³/min, and the average pure amount of extraction is 1.39 m³/min, which is much smaller than that in the (OPQRS) area.

As can be seen from Fig. 17: with the increase of extraction time, the gas extraction concentration in the (OPQRS) area rises continuously first, reaching a

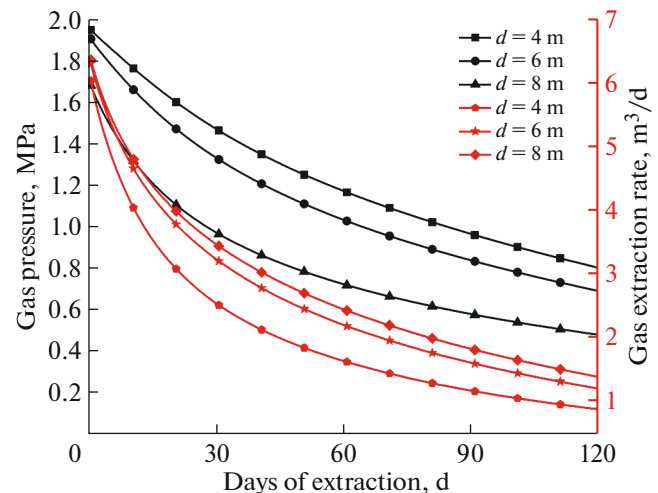


Fig. 15. Variation curves of gas pressure and extraction volume at the center of the borehole with different spacing.

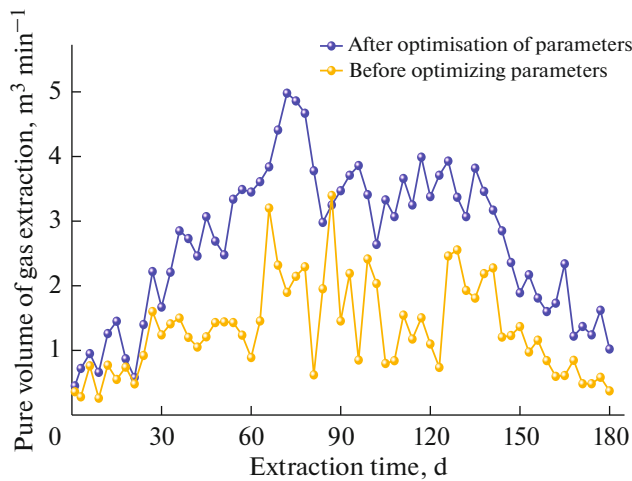


Fig. 16. Variation curve of pure volume of gas extraction.

peak of 53.5% after 72 days of extraction, and then declines continuously until the extraction concentration stabilizes at about 28% after 120 days, with an average extraction concentration of 36.1%, which is a good effect of gas extraction. The gas extraction concentration in the adjacent working face cascade borehole in the (OPQRS) area first rose continuously, reaching a peak of 35% on day 84, and then declined to 10–20% within a short time, with an average extraction concentration of 16.6% and a poor gas extraction effect. From the curves of pure gas extraction and extraction concentration, it can be seen that the gas extraction effect in the area after optimized extraction spacing (OPQRS) is significantly higher than that in the adjacent area.

DISCUSSION

The heat-fluid-solid coupling model of coal rock deformation field, gas seepage diffusion field and temperature field established in this paper is determined on the basis of mastering the characteristics of coal microscopic distribution, which is more in line with the characteristics of the coal seam. The model can verify the relationship between the working face gas extraction and seepage velocity, permeability change, and coal seam temperature, which not only helps to accurately grasp the coal seam gas transport law, but also simulates the work to optimize the extraction parameters such as borehole extraction hole diameter, spacing and row spacing. Coal mining enterprises can select a specific working face, substituting the field parameters for the debugging of the model, to ensure safe production while promoting the sustainable development of energy, which in turn guides the coal mining enterprises to carry out targeted on-site construction work.

From the related research, it is known that at the early stage of diffusion, the gas is rapidly discharged

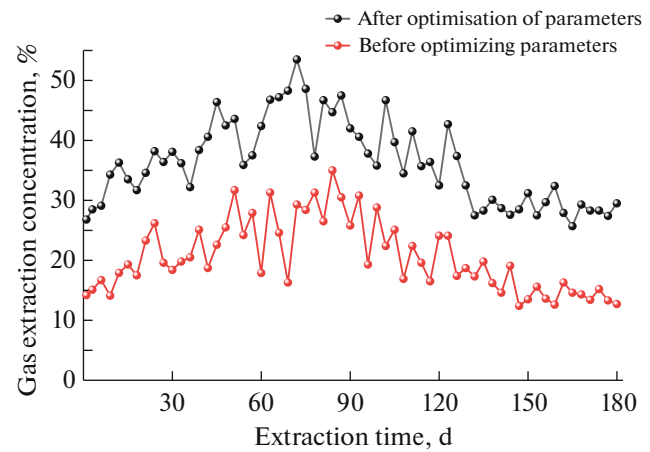


Fig. 17. Variation curve of gas extraction concentration.

from the large pores with larger diffusion coefficient, and at the later stage, it overflows from the small pores with smaller diffusion coefficient until it reaches the inside of the micropore, so the dynamic diffusion coefficient should be introduced in the numerical simulation depending on the attenuation change of gas diffusion [16]. The attenuation coefficient actually reflects the transfer process from the outer pores to the inner fissures of the coal, and the larger the value reflects the more difficult the transition between the pores-fissures. The movement of gas molecules between pore-fissure of coal body is related to the change of coal body permeability, and the spatial and temporal characteristics of coal body permeability evolution can be seen from Fig. 18: at the early stage of extraction, the influence of attenuation coefficient on coal body permeability is small, and the difference gradually starts to appear after 60d of extraction, and the difference of coal body permeability change becomes more and more obvious with the increase of extraction time, and the decrease of permeability decreases with the increase of attenuation coefficient.

As the change of permeability in the extraction process is determined by porosity and coal strain: with the progress of gas extraction, the gas pressure in the coal seam decreases, the effective stress in the coal seam increases, and the coal skeleton compresses while the coal matrix shrinks, resulting in corresponding changes in matrix porosity and fracture permeability. On the one hand, coal skeleton compression will lead to a decrease in coal porosity, which in turn causes a decrease in permeability; on the other hand, coal matrix contraction will cause the adsorbed gas to start desorption and produce matrix contraction effect, which makes the matrix porosity and permeability of coal gradually increase. The increase of attenuation coefficient indicates that the diffusion resistance of coal pore system increases, which makes the amount of gas flowing into the fissure decrease, and the coal matrix shrinkage effect keeps increasing and

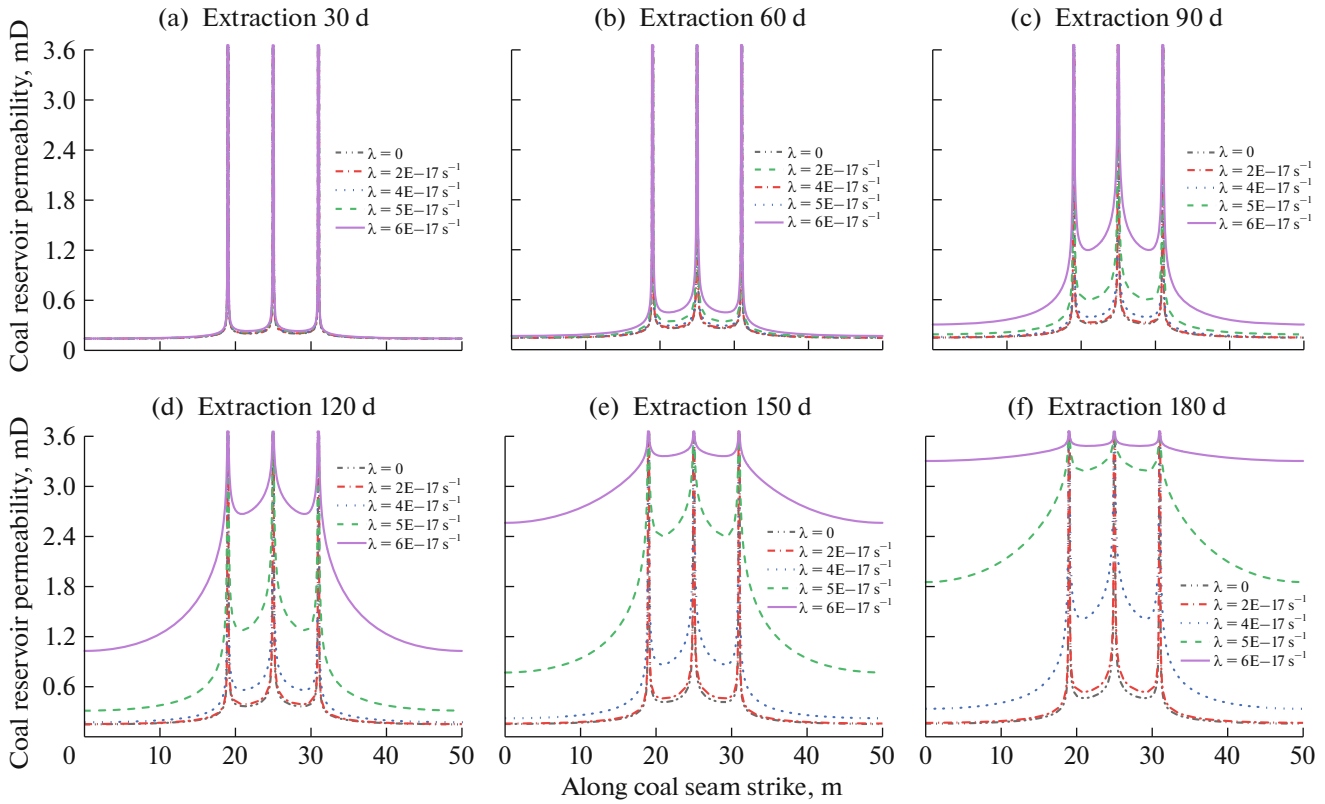


Fig. 18. Dynamics of coal permeability decay at different extraction times.

gradually dominates, so the permeability keeps increasing with the increase of time.

Before pre-pumping, the gas content of (OPQRS) area was between 5.23~7.52 m³/t, the maximum gas content was 7.52 m³/t, and the average gas content was 6.74 m³/t. After pre-pumping by drilling, the gas content of (OPQRS) area was between 2.3~3.76 m³/t, the maximum gas content was 3.76 m³/t, and the average gas content was 2.97 m³/t. After verification, the gas content of each borehole has dropped significantly, basically to less than 50% of the gas content before pre-pumping, meeting the pre-pumping requirements of OPQRS area at 172403 working face of Dashucun Mine.

According to the statistics, the spacing of drilling holes for gas extraction in the adjacent area of 172403 test working face (OPQRS) is 5 m, and the number of pre-sumping holes is 78. After optimization, the drilling spacing of the test working face is 6m, and the number of drilling works is 70, the number of drilling after optimization is reduced by 10%, and the formula for calculating the residual gas content of coal seam after pre-sumping is shown as follows:

$$W_{CY} = \frac{W_0 G - Q}{G} \quad (16)$$

Where W_{CY} is the residual gas content, m³/t; W_0 is the original gas content of the coal seam before pre-sumping, m³/t; G is the coal reserves of the evaluation unit, t; Q is the total extracted gas content, m³.

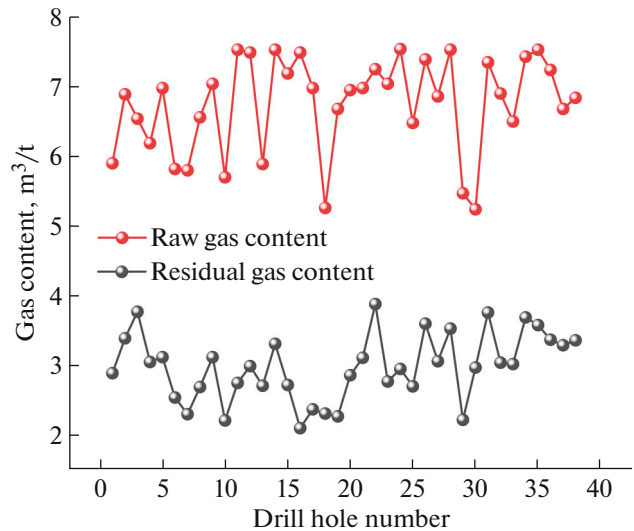


Fig. 19. Residual gas content in each borehole before and after pre-pumping.

The maximum residual gas content in the area after gas extraction (OPQRS) is 3.66 m³/t according to the mine production plan with a daily production of about 2000 t. The maximum residual gas content measured in the field after extraction is 3.76 m³/t, which is basically the same as the theoretical calculation and the field measurement results, with an error of only 2.7%, which is less than 5%.

The amount of gas that can be desorbed is calculated by the following equation:

$$W_{CC} = \frac{0.1ab}{1 + 0.1b} \times \frac{100 - A_d - M_{ad}}{100} \times \frac{1}{1 + 0.31M_{ad}} + \frac{\phi}{\gamma} \quad (17)$$

Where W_{CC} is the residual gas content at standard condition, m³/t; a, b is the adsorption constant; A_d is the ash content of the coal seam, %; M_{ad} is the moisture content of the coal seam, %; γ is the capacity of the coal, t/m³.

From the mine production plan, the daily output of working face is about 2000 t, (OPQRS) area W_{CY} is 3.66 m³/t, the maximum residual gas content is 3.76 m³/t, the maximum desorbable gas quantity of coal is calculated as $W_j = 1.86$ m³/t. This result is in line with the condition of daily output of coal mining working face as stipulated in the Provisional Regulations on Coal Mine Gas Extraction to Meet the Standard, the desorbable gas quantity before re-mining is less than or equal to 7 m³/t.

CONCLUSION

(1) The coal samples of Dashucun mine belong to anthracite coal with high coalization degree and high adsorption level to gas. The isothermal adsorption curves of the four groups of coal samples are all type IV curves, and the “hysteresis loop” is obvious. The microscopic pore size characteristics of the coal body were investigated through basic experiments, and the coupled heat-fluid-solid model of the coal seam was established, finally solved using COMSOL Multiphysics numerical simulation software.

(2) The temperature of the coal body is subject to gas desorption and heat dissipation and heat conduction, and shows a decreasing trend with the time of extraction, and the higher the temperature, the smaller the area of effective extraction area. The pressure difference between matrix and fissure makes the change of seepage rate and gas extraction divided into rapid rise, slow decline and stable stage. The larger the diffusion attenuation coefficient is, the weaker the matrix contraction effect is, resulting in a faster rate of decline in the permeability of the coal seam, a slower rate of gas seepage and a decrease in the amount of extraction.

(3) By analyzing the gas extraction volume and effective extraction radius of different hole diameters, it is determined that the hole diameter of 172403 working face is 114 mm. Combined with the residual pressure value of the superimposed effect of neighboring holes, the reasonable spacing of holes was determined to be 6 m. The optimized hole spacing was verified in the field. After field engineering verification, the optimized gas extraction efficiency is obviously improved, and the results of the study can promote the safe production of coal mines and the sustainable development of energy.

ACKNOWLEDGMENTS

This work was supported by the 14th Graduate Innovative Fund of Wuhan Institute of Technology (CX2022577), the Key Project of Hubei Province Education Department (D20201506), the National Natural Science Foundation of China Regional Fund (52064046), and the 2022 Hubei Master Teacher Studio.

CONFLICT OF INTEREST

The authors declare that they have no conflicts of interest.

REFERENCES

- Zhang, M., Lin, M., Zhu, H., Zhou, D., and Wang, L., *J. Loss Prev. Process Ind.*, 2018, vol. 55, p. 338. <https://doi.org/10.1016/j.jlp.2018.07.006>
- Minbo, Z., Jin, Y., Zichao, W., Ziyi, Z., Jianwei, C., and Qiuran, C., *Solid Fuel Chem.*, 2023, vol. 57, no. 4, p. 253. <https://doi.org/10.3103/S0361521923040158>
- Li, W., *J. Min. Saf. Eng.*, 2021, vol. 38, no. 1, p. 181. <https://doi.org/10.13545/j.cnki.jmse.2019.0522>
- Zhang, D., Zhang, M., Zhang, S., Wang, Z., Jin, Y., and Liu, R., *Sustainability*, 2023, vol. 15, no. 5, p. 4446. <https://doi.org/10.3390/su15054446>
- Li, Z., Ren, T., Li, X., Qiao, M., Yang, X., Tan, L., and Nie, B., *Int. J. Min. Sci. Technol.*, 2023, vol. 33, no. 4, p. 389. <https://doi.org/10.1016/j.ijmst.2022.12.006>
- Liu, X., Jia, X., Liu, W., Nie, B., Zhang, C., and Song, D., *Geoenergy Sci. Eng.*, 2023, vol. 225, p. 211691. <https://doi.org/10.1016/j.geoen.2023.211691>
- Liao, Z., Liu, X., Song, D., He, X., Nie, B., Yang, T., and Wang, L., *Nat. Resour. Res.*, 2021, vol. 30, p. 1613. <https://doi.org/10.1007/s11053-020-09782-5>
- Cheng, Y.P., Dong, J., Li, W., Chen, M.Y., Liu, K., and Zhao, W., *J. China Coal Soc.*, 2017, vol. 42, no. 6, p. 1466.
- Liu, J., Zhang, L., Wei, Y., and Wu, Z., *ACS Omega*, 2021, vol. 6, no. 50, p. 34920. <https://doi.org/10.1021/acsomega.1c05574>
- Zhang, H., Cheng, Y., Deng, C., Shu, L., Pan, Z., Yuan, L., Wang, L., and Liu, Q., *Rock Mech. Rock Eng.*, 2022, vol. 55, no. 2, p. 885. <https://doi.org/10.1007/s00603-021-02691-w>

11. Yue, G., Liu, H., Yue, J., Li, M., and Liang, W., *Energy Sci. Eng.*, 2019, vol. 7, no. 3, p. 694.
<https://doi.org/10.1002/ese3.285>
12. Wu, K., Shi, S., Lu, Y., Li, H., and Li, M., *Geofluids*, 2021, vol. 2021, p. 1.
<https://doi.org/10.1155/2021/8147366>
13. Yan, J., Zhang, M., Zhang, W., and Kang, Q., *Sustainability*, 2023, vol. 15, no. 10, p. 8409.
<https://doi.org/10.3390/su15108409>
14. Xu, C., Qin, L., Wang, K., Sun, H., and Cao, M., *Energy Sci. Eng.*, 2021, vol. 9, no. 4, p. 509.
<https://doi.org/10.1002/ese3.871>
15. Lin, B., Liu, T., and Yang, W., *J. China Univ. Min. Technol.*, 2018, vol. 47, no. 1, p. 32.
16. Zhang, C., *MSc Thesis*, Anhui Univ. of Science and Technology, 2020.
17. Ding, W., *MSc Thesis*, Henan Polytechnic Univ., 2016.
18. Zhang, M., Wang, Z., Wang, L., Zhang, Z., Zhang, D., and Li, C., *Combust. Theory Modell.*, 2023, vol. 27, no. 1, p. 118.
<https://doi.org/10.1080/13647830.2022.2153742>
19. Bo, L., Donghui, S., and Lulu, Z., *Coal Sci. Technol.*, 2016, vol. 44, no. 8, p. 121.
20. Zhang, M., Wang, Z., Yan, J., Li, C., Zhong, Z., Qian, Z., and Liu, R., *Coal Eng.*, 2023, vol. 55, no. 5, p. 116.
21. Chang, B., Chen, J., Liu, J., Sun, H., and Yan, R., *J. Xi'an Univ. Sci. Technol.*, 2016, vol. 36, no. 6, p. 793.
<https://doi.org/10.13800/j.cnki.xakjdxsb.2016.0606>
22. Tao, Y., *Saf. Coal Mines*, 2012, vol. 43, no. 2, p. 9.
<https://doi.org/10.13347/j.cnki.mkaq.2012.02.013>
23. Zhang, M., Yan, J., Zhong, Z., Wang, Z., Qian, Z., and Li, C., *Min. Res. Dev.*, 2023, vol. 43, no. 6, p. 134.
<https://doi.org/10.13827/j.cnki.kyyk.2023.06.005>
24. Zhang, P., *Energy Environ. Sci.*, 2021, vol. 43, no. 5, p. 29.
<https://doi.org/10.19389/j.cnki.1003-0506.2021.05.006>
25. Hao, J., Liang, B., Sun, W., Shi, Z., Shi, Y., and Zhao, H., *J. Min. Saf. Eng.*, 2022, vol. 39, no. 5, p. 1051.
26. Lu, S., Zhang, Y., Sa, Z., Si, S., Shu, L., and Wang, L., *Energy Sci. Eng.*, 2019, vol. 7, no. 4, p. 1352.
<https://doi.org/10.1002/ese3.355>
27. Zhang, H., Cheng, Y., Liu, Q., Yuan, L., Dong, J., Wang, L., Qi, Y., and Wang, W., *J. Nat. Gas Sci. Eng.*, 2017, vol. 46, p. 498.
<https://doi.org/10.1016/j.jngse.2017.08.022>
28. Lu, W. and Huang, B., *Adsorpt. Sci. Technol.*, 2020, vol. 38, nos. 3–4, p. 127.
<https://doi.org/10.1177/0263617420919247>
29. Zhao, D., Liu, J., and Pan, J.T., *J. Loss Prev. Process Ind.*, 2018, vol. 54, p. 266.
<https://doi.org/10.1016/j.jlp.2018.04.013>
30. Hu, S., Liu, X., and Li, X., *Processes*, 2020, vol. 8, no. 2, p. 254.
<https://doi.org/10.3390/pr8020254>
31. Wang, X., Zhou, H., Zhang, L., Preusse, A., Xie, S., and Hou, W., *Geomech. Geophys. Geo-Energy Geo-Res.*, 2022, vol. 8, no. 5, p. 149.
<https://doi.org/10.1007/s40948-022-00464-5>